RSC Advances

PAPER

View Article Online
View Journal | View Issue

Cite this: *RSC Adv.*, 2024, **14**, 7303

Preparation of an innovative series of respiratory nano-filters using polystyrene fibrous films containing KCC-1 dendrimer and ZnO nanostructures for environmental assessment of SO_2, NO_2 and CO_2†

Farzaneh Edrisi,[a] Mehdi Mahmoudian*[ab] and Nasrin Shadjou *[ab]

Air pollution has become a major challenge that threatens human health. The use of respiratory filters is one of the proposed solutions. In this study, using polystyrene (PS) fibers and various nanomaterials, improved respiratory filters were fabricated to remove air pollutants. In this context, ZnO nanoparticles (ZnO NPs) integrated into dendritic structures of KCC-1 silica were used to improve the filters' ability to absorb pollutants. For the first time, the removal of gasses by modified filters with a novel polymeric nanocomposite (PS/ZnO-KCC-1) stabilized on the surface of respiratory filters was investigated. Moreover, two different methods including stabilized- and solution-based techniques were used to prepare the filters with different amounts of ZnO NPs and their efficiency was evaluated. All synthesized nanocomposites and developed filters were characterized by FT-IR, FESEM, TGA and XRD methods. The successful stabilization of nanostructures on the fibers was proved and the performance of the fibers was investigated with some tests, such as pressure drop and removal of suspended particles and CO_2 (89%), NO_2 (86%), and SO_2 (83%) gases. PS/KCC-1-ZnO (5%) has better performance than other prepared fibers. The results showed that the removal of suspended particles in the filter containing ZnO and KCC-1 (M5) nanostructures was improved by 18% compared to the filter consisting of polystyrene fibers. The pressure drop increased with the addition of nanostructures and reached 180 Pa in the M5 filter. The filter containing ZnO NPs showed antibacterial activity against *Staphylococcus* (*S.*) *aureus* and *Escherichia* (*E.*) *coli* as Gram-positive and Gram-negative model bacteria using the Agar disk-diffusion method. Based on the results, the use of improved respiratory filters is recommended as an effective solution for combating air pollution and protecting human health.

Received 7th January 2024
Accepted 26th February 2024

DOI: 10.1039/d4ra00176a

rsc.li/rsc-advances

1. Introduction

Pollution caused by human activities is one of the significant environmental problems in the world. In recent years, air pollution stemming from the significant expansion of industrial and agricultural companies, exhaust fumes from road transportation, and unrestrained energy consumption has had a significant impact on the health and life of people worldwide. In most industrialized developed countries, the concentration of air pollutants is higher than the level set by the World Health Organization, leading to severe problems and risks.[1] SO_2, CO_2, and NO_2 are the three primary air pollutants that can cause serious health problems when exposed to them. Polluted air can enter the lungs directly and cause respiratory and heart problems, including asthma.[2] On the other hand, the emergence of infectious and contagious diseases in recent decades poses a severe threat to human health. Therefore, due to the increase in air pollutants and the prevalence of contagious diseases, the use of respiratory masks is considered mandatory.[3]

Any covering or device that covers part of the face is called a mask. Masks are considered personal protective equipment that prevents the entry of pollutants in the air into the respiratory system through the nose, mouth, lungs, *etc.* Nowadays, researchers are working to improve the efficiency of respiratory mask filters.[4] The efficiency of conventional filters is almost 99.97% for large particles, but their efficiency for particles smaller than 2.5 micrometers is very low. On the other hand, the masks available in the market have a problem of losing static electricity when used for a long time or exposed to moisture, which limits their filtration efficiency. In recent studies, modifying mask filters and producing new types of masks with better efficiency using nanotechnology has received much attention.[5]

[a]*Faculty of Chemistry, Department of Nanotechnology, Urmia University, Urmia, Iran. E-mail: m.mahmoudian@urmia.ac.ir; n.shadjou@urmia.ac.ir; Tel: +98 44 32752741*

[b]*Nanotechnology Research Center, Urmia University, Urmia, Iran*

† Electronic supplementary information (ESI) available. See DOI: https://doi.org/10.1039/d4ra00176a

Fibers of materials with unique properties, such as very high surface-to-volume ratio, small diameter, the ability to form porous layers with tiny pores, and high flexibility, are useable in a wide range of fields, including the production of membranes, tissue engineering, sensors, drug delivery systems, and wound dressings.[6]

The electrospinning process is the most important method for producing fibers due to the use of a wide range of polymers, ease of operation, low cost, high porosity, production of extremely lightweight and thin fibers with a high surface-to-volume ratio, and the ability to control pores. It can be used in the production of natural and synthetic polymer fibers.[7] Natural polymer materials such as hyaluronic acid, gelatin, chitosan, elastin, silk, and wheat protein can be used in addition to synthetic polymer materials such as polylactic acid, polyethylene terephthalate, caprolactone, polylactic-*co*-glycolic acid, polyvinyl acetate, polystyrene, and polyvinyl alcohol. The effective parameters on electrospinning fibers can generally be classified into parameters related to the polymer solution (molecular weight, solution viscosity, surface tension, electrical conductivity, and dielectric effect), parameters related to operational conditions (applied voltage, collector effect, needle hole diameter, and distance between needle tip and collector), and environmental conditions (temperature, humidity, pressure).[8]

In recent studies, nanomaterials have been used to improve the performance of fibers. Porous materials have nano-sized cavities, which give them a high surface-to-volume ratio, high permeability, good selectivity, and thermal and acoustic resistance. Silica is one of the most common materials used to make mesoporous structures with various morphologies. The synthesis of mesoporous silica is simple and inexpensive, and it can be prepared on an industrial scale with simple processes.[9] KCC-1 is a type of porous silica with a three-dimensional dendrimer structure that makes it a perfect substrate and carrier. KCC-1 can be modified with various functional groups and is used in many applications, including catalysts, photocatalysts, energy absorption in solar cells, CO_2 capture, targeted drug delivery, photothermal therapy, and imaging.[10] On the other hand, ZnO NPs are highly sought after due to their unique optical, electronic, and piezoelectric properties, as well as their high chemical stability, low dielectric constant, high catalytic activity, and absorption of infrared and ultraviolet light. Most importantly, they possess antibacterial properties, making them very useful in industry.[11]

Research has been conducted on the use of nanocomposite fibers in respiratory masks. Sanaw *et al.* compared the efficiency of nanofibers as a mask filter with a melt-blown layer in 2020. They investigated the effect of ethanol on layers and found that the resistance of the nanofiber filter to moisture improved.[12] They investigated the effect of ethanol on layers and found that the resistance of the nanofiber filter to moisture improved. In another study by Dong Wang *et al.* in 2021, poly-styrene nanofiber composite filters were used on N95 masks, resulting in increased filtration efficiency and reduced pressure drop.[13] Tang and Han used poly-styrene nanofiber composites containing silica nanoparticles to fabricate filters in 2021, and the results showed high filtration and permeability of the filters.[14]

To effectively eliminate harmful chemical compounds from environmental samples, it is crucial to employ efficient methods. One suggested approach is the adoption of respiratory filters. This research endeavors to address the shortcomings of previous techniques, such as low removal efficiency, utilization of hazardous materials for the removal process, and the high cost of substrates required for the elimination of specific air pollutants such as SO_2, CO_2, and NO_2. The focus is on investigating the enhanced removal of gases through modified filters incorporating a novel polymeric nanocomposite (PS/ZnO-KCC-1) immobilized on the respirator filter surface. The ultimate goal is to enhance the capacity of existing respiratory masks to eliminate gases and therefore bolster their effectiveness in combatting air pollution. The study involves examining the impact of electro-spun nanocomposite fibers, comprising of polystyrene with KCC-1 and ZnO (PS/KCC-1, ZnO), employed to create a layer within these masks, particularly in relation to their absorption and antibacterial properties. The selection of polystyrene as the polymeric material is rooted in its cost-effectiveness and widespread availability.

2. Experimental

2.1. Materials

Cetyltrimethylammonium bromide (CTAB), zinc nitrate hexahydrate ($Zn(NO_3)_2 \cdot 6H_2O$), cyclohexane (C_6H_{12}), hexanol ($C_6H_{13}OH$), ethanol (C_2H_5OH) and polystyrene was obtained from d from Merck, Germany. Tetraethyl orthosilicate (TEOS) and dimethylformamide (DMF) were purchased from Sigma-Aldrich (St. Louis, Mssouri, United States).

2.2. Synthesis of KCC-1

KCC-1 was synthesis according to the methods which was reported by Soleymani *et al.*[15] Initially, 1 g of CTAB was dissolved in 10 mL of water, and 0.6 g of urea were added. Then, 2 g of TEOS, 30 mL of cyclohexane, and 1.5 mL of hexanol were introduced into the solution, homogenized for 30 minutes. The mixture was heated to 80 °C for 4 h, refluxed for 24 h, and cooled to collect KCC-1 in white powder form. The powder was washed with water and ethanol and dried overnight at 60 °C. A calcination process at 550 °C for 6 h removed any remaining CTAB. CTAB served as a soft template, while urea facilitated hydrolysis and generated a negatively charged silicate structure during KCC-1 synthesis. Scheme 1 indicated chemical structure of KCC-1.

2.3. Synthesis of ZnO NPs

The method available in the reference was used to prepare ZnO NPs.[16] ZnO NPs were synthesized using the sol–gel method. Polyvinyl alcohol (PVA) was dissolved in double distilled water, and zinc nitrate hexahydrate was dissolved in a separate solution. The zinc nitrate hexahydrate solution was added dropwise into the PVA solution at 70 °C with constant stirring for 2 h until a gel-like substance formed. The resulting gel was dried in an oven at 160 °C for 12 h and then calcined in an open-air muffle furnace at temperatures ranging from 400–600 °C for 8 h. The exact process was repeated to prepare ZnO NPs with PVA concentrations of 1.89, 2.27, and 3.34 M at a temperature of 400 °C.

2.4. Preparation of fibrous filters

To prepare a polystyrene fiber, 2 g of PS was dissolved into 8 mL of DMF under stirring for 5 h. Fibers membranes were made using an electrospinning apparatus. Which consists of a high voltage (HV) power supply, drum collector, syringe pump, and synthesis chamber with a controlled environment. The PS fiber membranes were prepared under a constant voltage of 24 kV and a spinning distance of 15 cm. The flow rate of the PS/DMF solutions loaded into a 15 mL syringe was precisely controlled using a syringe pump at a constant flow rate of 4 mL h^{-1}.

2.5. Preparation of fibrous nanocomposite filters

Two different methods were used to insert KCC-1 and ZnO NPs into the structure of nanofibers fixed on the mask (Scheme 2).

In the solution method, KCC-1 and ZnONPs were added to the polymer solution at concentrations of 1, 5 and 7 wt%, was stirred at room temperature for 30 min, then it was used to prepare fibers. However, in the stabilization method, KCC-1 and ZnONPs at concentrations of 1, 5 and 7 wt% were dispersed in 30 mL distilled water, was stirred at room temperature for 2 h and then the dispersed NPs were stabilization on the fibers with a vacuum pump. The different compositions of prepared formulations are tabulated in Table 1.

2.6. Instruments

The Field Emission Scanning Electron Microscopy (FESEM) images and Energy Dispersive X-ray (EDX) were recorded with FEG-SEM MIRA3 TESCAN, Czech Republic at 1000 kV. Spectra were obtained by Thermo-Nicolet Nexus 670 FT-IR instrument (Thermo Fisher Scientific, Waltham, MA, USA). The X-ray Diffractometer Infrared, used to study the crystallinity of the NPs, was X'PertPro, Holland radiation (30 kV, 15 mA). The measurement was conducted at 2 theta angles between 10 and 80. Thermal gravimetric analysis (TGA) was recorded by SDT Q600, US. PM particle number concentration was detected by Purific Y09-301, China.

2.7. Air filtration performance

Air filtration testing was performed to measure the filter pressure drop, remove airborne pollutants below 2.5 microns, and eliminate gases such as CO_2, SO_2, and NO_2. The components of this device include an air supply, an airflow controller, a filter

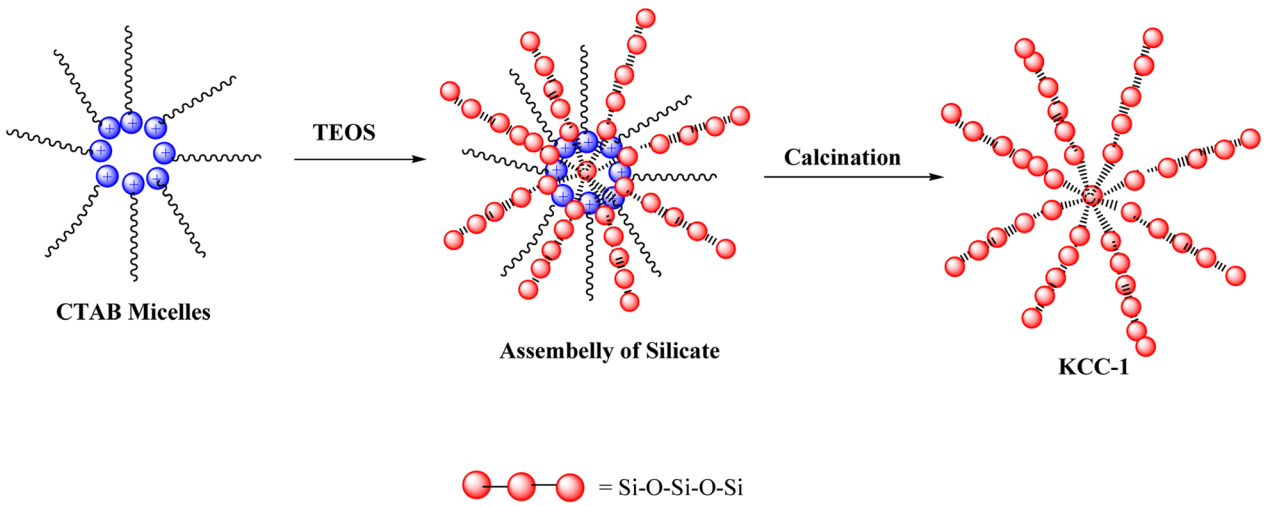

Scheme 1 Chemical structure of KCC-1.

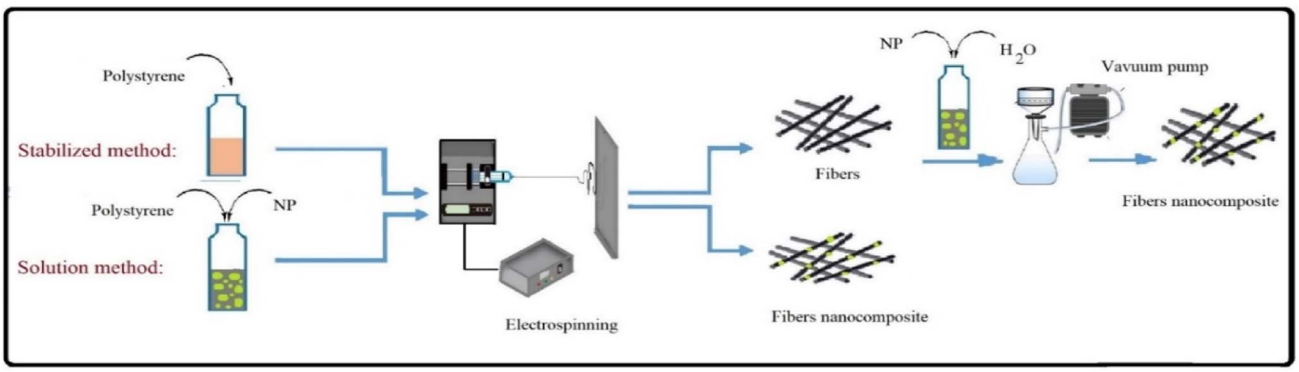

Scheme 2 Preparation processes of fibers nanocomposite.

Table 1 The properties of the fibers precursor solution at different concentrations

Filter structures	Solution method	Stabilized method
PS fibers	2 g PS, 8 mL DMF	2 g PS, 8 mL DMF
PS/KCC-1 1% fibers	2 g PS, 0.01 g KCC-1, 8 mL DMF	(1) 2 g PS, 8 mL DMF (2) 0.01 g KCC-1, 30 mL H_2O
PS/KCC-1 5% fibers	2 g PS, 0.05 g KCC-1, 8 mL DMF	(1) 2 g PS, 8 mL DMF (2) 0.05 g KCC-1, 30 mL H_2O
PS/KCC-1 7% fibers	2 g PS, 0.07 g KCC-1, 8 mL DMF	(1) 2 g PS, 8 mL DMF (2) 0.07 g KCC-1, 30 mL H_2O
PS/ZnO 5% fibers	2 g PS, 0.05 g ZnO, 8 mL DMF	(1) 2 g PS, 8 mL DMF (2) 0.05 g ZnO, 30 mL H_2O
PS/KCC-1, ZnO 5% fibers	2 g PS, 0.05 g KCC-1, 0.05 g ZnO, 8 mL DMF	(1) 2 g PS, 8 mL DMF (2) 0.05 g KCC-1, 0.05 g ZnO, 30 mL H_2O

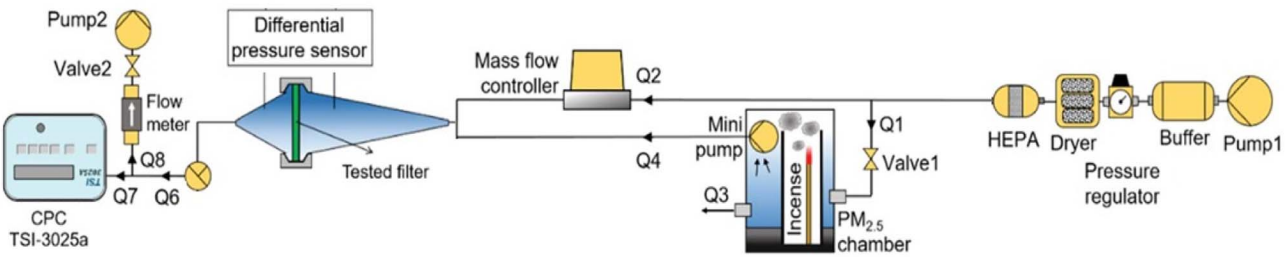

Scheme 3 A schematic diagram of the air filter test system.

holder, an artificial filter holder, a differential pressure sensor, a CPC particle counter, and a PM2.5 chamber. In this chamber, a type of fuel has been burned and the produced suspended particles are being used to evaluate the performance of particle removal. A compressor pump equipped with a buffer, pressure regulator, dryer, and HEPA filter provides clean and dry air for filter testing. The airflow is transferred from the compressor pump to a mass flow controller and a PM2.5 chamber. The airflow passing through the mass flow controller dilutes the particle-laden air stream, and the particle concentration is adjusted in the filter holders. Inside the PM2.5 chamber, a small pump delivers the air to the filter holders and releases excess flow pressure from an outlet inside the chamber. The filter sample is placed in the holder, and the pressure drop is measured using a differential pressure sensor connected to the holder. The particle concentration of each filter output is measured using a CPC. Portable gas detectors (SBKDPT) were used to measure the pollutant gas concentration in the inlet and outlet air. In this study, the temperature was 25 °C, the flow rate is 0.3 L min^{-1} and operation time was 1 h. The components of the device are illustrated in Scheme 3.

2.8. Antibacterial tests

The antibacterial activity of electro-spun PS fiber was evaluated in the presence or absence of ZnO NPs. The pathogens used in this test were *Staphylococcus* (*S.*) *aureus* and *Escherichia* (*E.*) *coli* as Gram-positive and Gram-negative model bacteria, respectively. The Fiber were cut into 1 × 1 cm^2, sterilized under UV light for 2 h and were exposed to standardized bacterial suspensions. Bacterial suspension diluted in TSB without fiber at 3 h was considered as control samples. All experiments were repeated in triplicate. Subsequently, the plates were incubated for 24 h, and at 37 °C and antibacterial activity was investigated.

3. Results and discussion

3.1. Characterization

3.1.1. Characterization of synthesized NPs and nanocomposite. The FT-IR spectra of the synthesized KCC-1 and ZnO are shown in Fig. 1. In the FT-IR spectrum of KCC-1 NPs, the bending and symmetric and asymmetric vibration of Si–O functional group were indicated by peaks at 439, 1100 and 799 cm^{-1}, respectively.[17] The characteristic peak of ZnO NPs appeared at around 568 cm^{-1} was related to Zn–O bond. The broad peak around 3450 cm^{-1} was assigned to the O–H stretching mode of hydroxyl group and the peak at 1652 cm^{-1} (bending) is due to asymmetrical stretching of the zinc carboxylate.[18]

FESEM was used to determine the morphology of the KCC-1 and ZnO NPs. Fig. 2 shows the FESEM images of the KCC-1 and ZnO NPs. Based on these images, the dimeric structures of KCC-1 NPS were observed in the samples. Also, FESEM images of ZnO NPs, show spherical shape of these NPs. The size of the prepared materials is less than 100 nanometers. By zooming in with a magnification of one micrometer, it is possible to observe the clusters formed by these NPs, indicating their high activity and tendency to agglomerate.

The elemental composition of the KCC-1 and ZnO NPs samples was determined by EDX analysis. The results are given

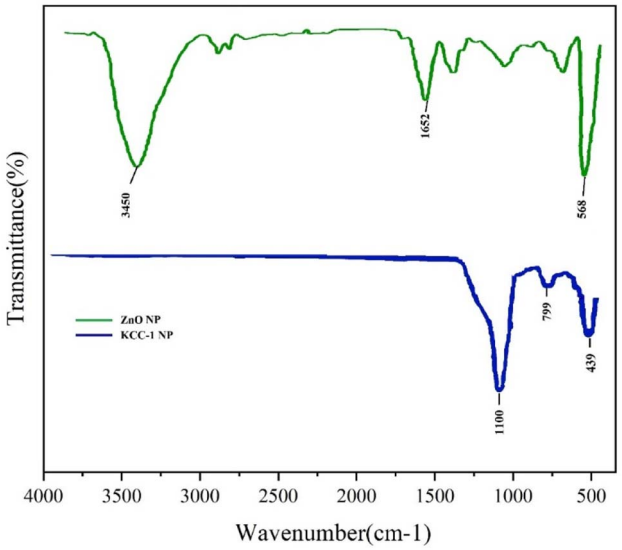

Fig. 1 FT-IR spectra of KCC-1 and ZnO NPs.

in Fig. 2. The EDX spectrum for KCC-1 revealed that the as-prepared products are contained Si, C, N and O, respectively. The EDX spectrum for ZnO, revealed that the as-prepared products are contained Zn, O.

XRD analysis was used to determine the crystalline phase of the samples. The XRD patterns of the synthesized KCC-1 and ZnONPs are shown in Fig. S1 (see ESI†). According to the XRD pattern for KCC-1, peaks centered at $2\theta \approx 10$–18 represent silica's porous structures, peaks centered at $2\theta \approx 20°$ represent the amorphous siliceous phase in the KCC-1.[19] Xray diffraction pattern of ZnO NPs, had characteristic diffraction peaks located at $2\theta = 31°$, 34.5°, 36°, 47°, 56.5°, 62°, 68°, and 69°, have been keenly indexed as hexagonal wurtzite phase of ZnO.[20] Also, the particle size obtained for ZnO NPs using the Scherrer equation (about 43 nm)[21] agreed with the FESEM image.

3.1.2. Characterization of synthesized nanocomposite fibers. Fig. S2 (see ESI†) shows the FT-IR spectra of the electrospun PS fibers and PS-nanocomposite fibers. The principal peaks of PS fibers including C–H stretching vibration of benzene ring, overtone and combination bands, ring stretching, mono-substituted ring, C–H out-of-plane bending can be seen

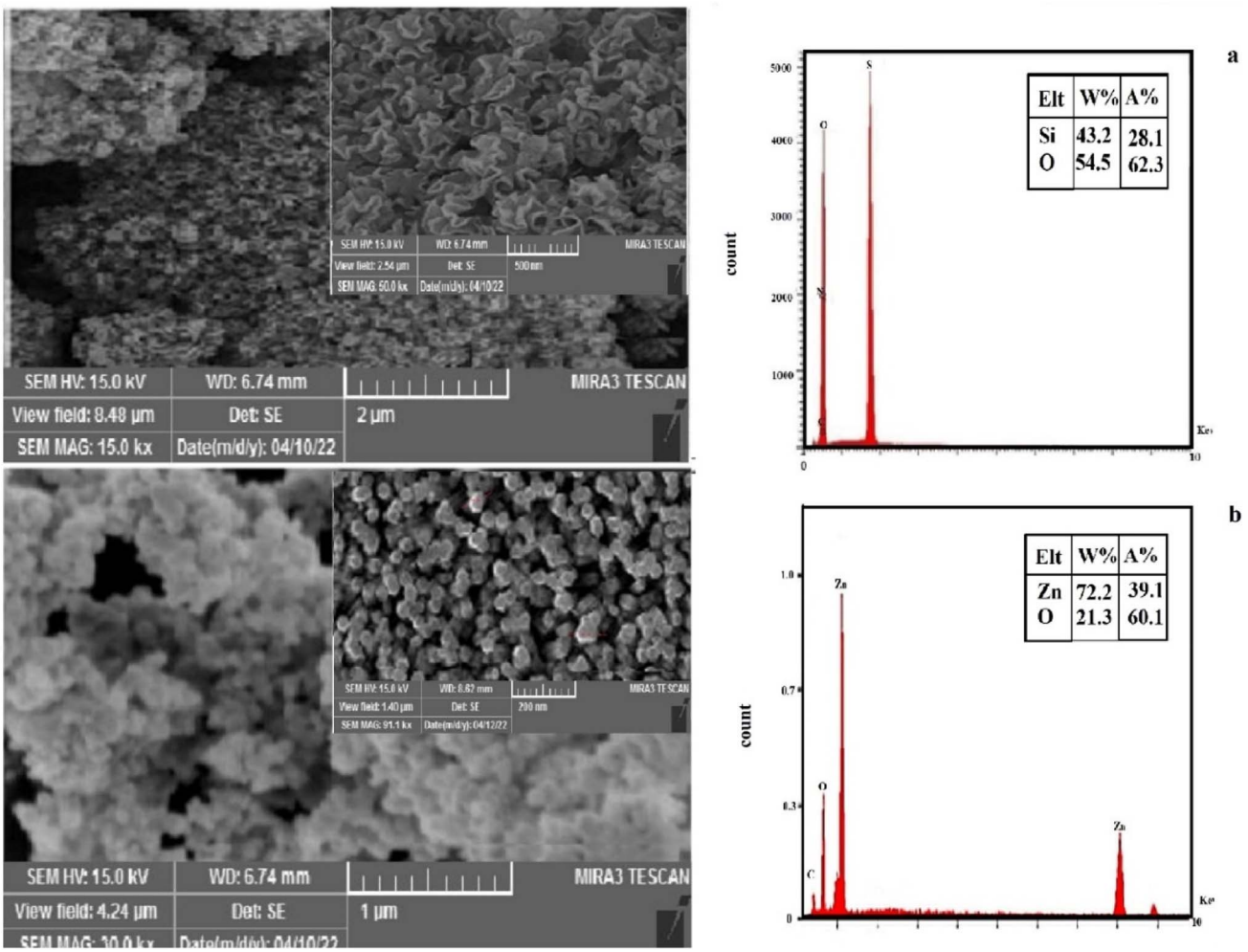

Fig. 2 FESEM-EDS of (a) KCC-1 NPs, (b) ZnO NPs.

at 3030, 1875, 1595 and 1447, 753, and 692 cm^{-1}, respectively.[22] In the FT-IR spectrum of PS/KCC-1 fibers, the principal peaks, Si–O symmetric and Si–O asymmetric stretching, appeared at 805–813, 1158–1163 cm^{-1}.[17] The stretching vibration of Zn–O bond appeared at around 440–450 cm^{-1}.[18] Considering both figures for both methods, it can be seen that the additive stabilization method did not change the spectral behavior.

Fig. 3 shows the FESEM image of the PS and PS-nanocomposite fibers. As can be seen, the PS fibers, were very uniform and smooth with an average diameter of about 1–1.6 μm. The smooth and uniform surface of polystyrene fibers has turned into a non-uniform surface with the addition of NPs. The products obtained in both methods do not differ much from the morphological point of view. Fig. 3b and c shows the FESEM of the PS/KCC-1 fiber's solution. The surface fibers are non-uniform and have small protrusions visible on their surface. These protrusions are attributed to the nanostructures fixed on the surface of the fibers. The fiber diameter obtained in this sample is within the range of polystyrene fibers. Fig. 3e and f shows the FESEM of the PS/KCC-1, ZnO fiber's. The morphology of uniform and elongated fibers can be observed, which may be due to the excellent dispersion of NPs within the polystyrene fiber solution. In this sample, the presence of fixed nanostructures in the form of protrusions on the fibers can also be detected.

To further ensure the dispersion of nanostructures on the polystyrene fiber filters, samples containing KCC-1 and ZnONPs were analyzed using EDS (Energy-Dispersive X-ray Spectroscopy). The results of this analysis, along with the weight percentage of elements, are shown in Fig. S3 (see ESI†). In the pure polystyrene fiber structure, the presence of carbon was identified. Based on the presented diagram for the KCC-1 and ZnO nanocomposite fibers, elements such as zinc, silicon, oxygen, and carbon can be confirmed. Silicon and oxygen elements were also present in the EDS diagram of the KCC-1 nanostructures, indicating the successful fixation of the desired structures in the polystyrene matrix.

The structure of pure polystyrene fiber and polystyrene nanocomposite fibers containing KCC-1 and ZnONPs was investigated using XRD, and the observed patterns are visible in Fig. S4 (see ESI†). In the XRD diagram of pure polystyrene fibers, a broad band at $2\theta = 20$ was visible due to the amorphous

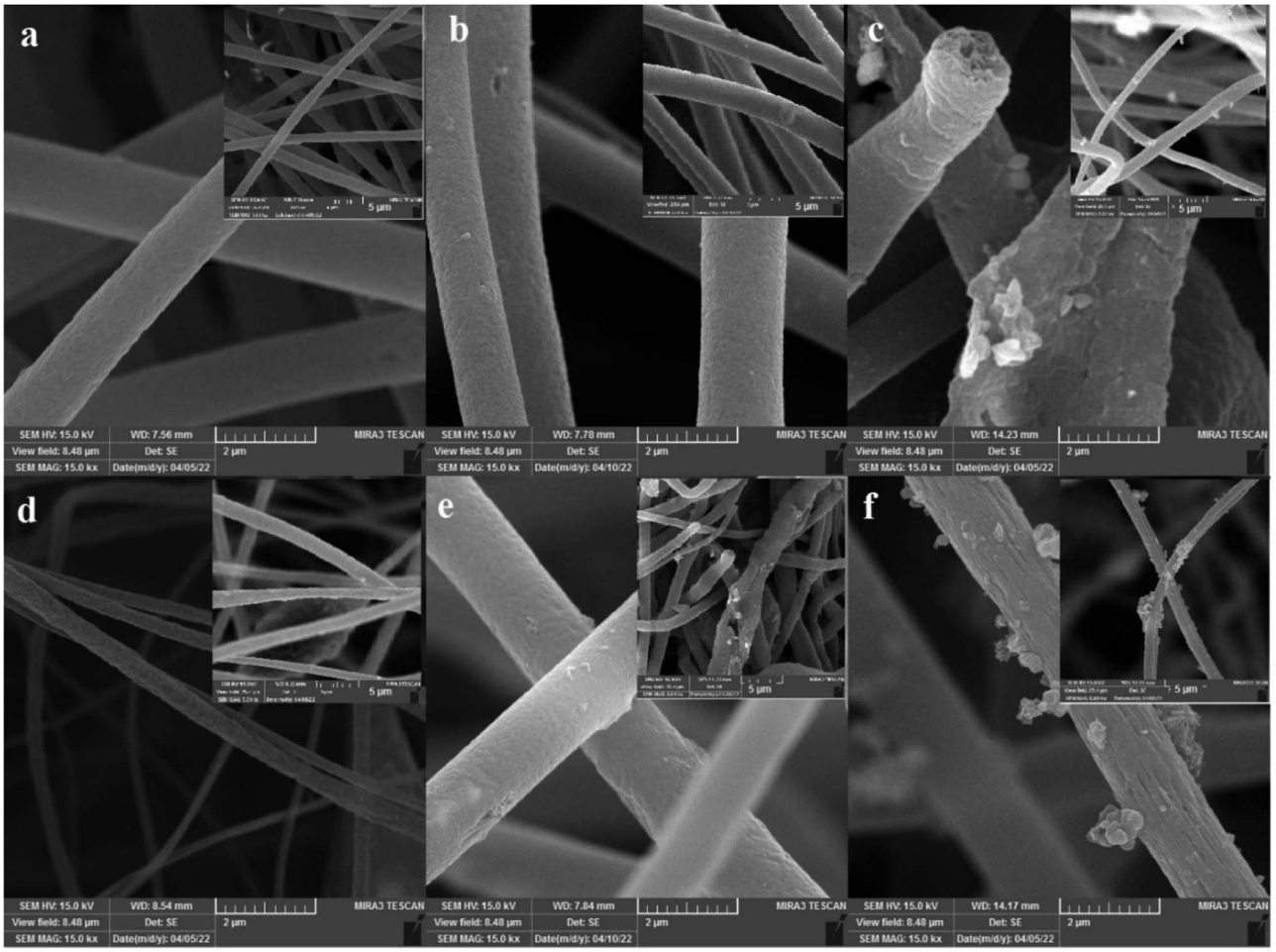

Fig. 3 FESEM images of (a) PS fibers, (b) PS/KCC-1 1% fibers solution, (c) PS/KCC-1 7% fibers solution. (d) PS/ZnO 5% fibers stabilize, (e) PS/KCC-1, ZnO 5% fibers solution, (f) PS/KCC-1, ZnO 5% fibers stabilize.

structure of polystyrene.[23] In the XRD diagram of KCC-1-containing nanocomposite fibers, the characteristic peaks of these nanostructures appeared in the XRD pattern which, confirmed their presence in the polystyrene matrix.[18] Also, in the XRD diagram of ZnO-containing nanocomposite fibers, the appearance of narrow bands at around 31, 36, and 47, which were observed with low intensity, was related to the hexagonal crystal structure of ZnO.[20] One point that can be seen in the XRD diagrams containing NPs is the appearance of sharp bands in the 2θ range between 10 and 20°, indicating that the presence of NPS has also changed the crystallization behavior of polystyrene.

The TGA curves of the PS and PS/KCC-1, ZnO nanocomposite fibers are shown in Fig. S5 (see ESI†). The results showed that pure polystyrene fibers have good thermal stability, and the remaining ash content is nearly zero percent. The addition of KCC-1 has caused degradation to begin at lower temperatures. This trend has also been observed in nanocomposite samples containing ZnONPs and ZnO-KCC-1 hybrids, indicating that the presence of NPs reduced the thermal stability of the samples. This decrease has been observed in other studies, due to the catalytic role of NPs in degradation processes.[24] On the other hand, it is observed that the ash content has increased in samples containing ZnONPs, which was justifiable considering the mineral nature of the NPS.

3.2. Air filtration performance

3.2.1. Polymeric membrane (PM) removal efficiency. The graph in Fig. 4 shows the performance of removing suspended particles in the air by composite fibers prepared by two methods of solution and stabilization. The performance of a three-layer mask (one layer of melt-blown and two layers of spun bond) was only 47%, while in a modified filter with pure polystyrene fibers, the efficiency was 81%, and in nanocomposite filters, this percentage increases with the addition of NPs. The performance of the fibers prepared by the stabilization method was better than the solution method, the highest performance was related to fibers containing stabilized KCC-1 and ZnONPs, and this filter was able to remove 99% of suspended particles. The significant increase in the removal efficiency of the modified polystyrene fiber filter was attributed to the large number of gaps and cavities created by the nanofibers and structures on the surface of the regular mask film. The suspended particles in the air were trapped in these gaps during passage through the filter and captured by the filter. In filters where nanostructures such as KCC-1 and ZnONPs were stabilized on the fibers, the separation mechanism can be different so that the stabilized nanostructures form a compact layer on the surface of the filter and prevent the passage of fine suspended particles. Fine particles that pass through this layer can be captured by the gaps between the polymer fibers. Therefore, the higher efficiency of these filters was justifiable.

3.2.2. Pressure drop test. Pressure drop is one of the most critical performance characteristics of filters, and it increases with the reduction of pores and porosity in filters. Pressure drop determines the flow rate through the filter, and excessive

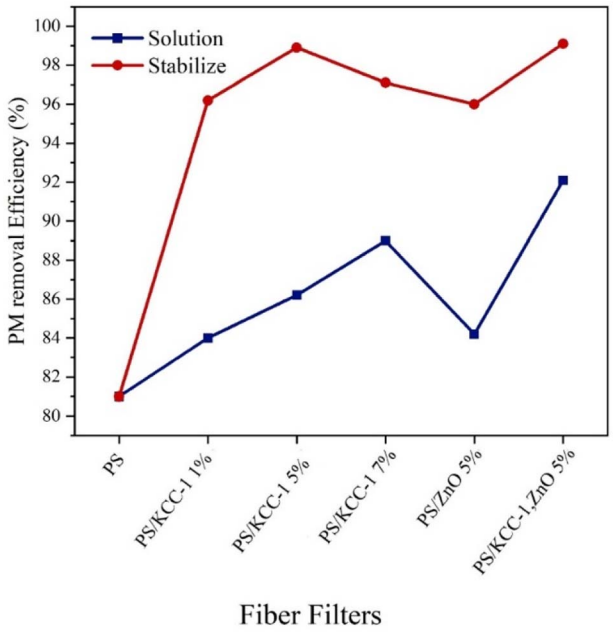

Fig. 4 PM removal efficiency of PS fibers and PS-nanocomposite fibers.

increase is not desirable. Fig. 5 shows the pressure drop of modified filters made of polystyrene and nanocomposite fibers. The pressure drop for the regular mask was 43.2 Pa, and for the modified filter with pure polystyrene fibers, this value was 52.4 Pa. The presence of polystyrene fibers on the surface of the filter reduced the flow rate and caused a higher pressure drop. The presence of NPS in filters containing nanocomposite fibers has increased the pressure drop to a greater extent. It was observed that with an increase in the percentage of NPS, the pressure drops also increased and reached the highest value (180 Pa) in

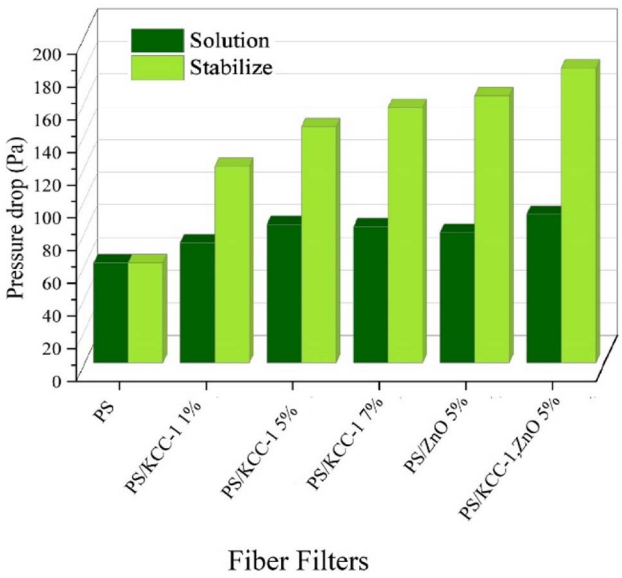

Fig. 5 Pressure drops of PS fibers and PS-nanocomposite fibers.

the sample containing both KCC-1 and ZnO NPs. As mentioned in the explanation of removing suspended particles under 2.5 microns, the attachment of particles to fibers created a compact layer on the surface of the filter, which restricted the passage of airflow and, as a result, increased the pressure drop on both sides of the filter. Due to the method of stabilizing NPs on the surface of fibrous filters, these NPs were deposited on the fibers, and the inter-fiber space was reduced. As a result, an obstacle was created to prevent air passage, and the pressure drop increased on both sides of the filter. This pressure drop, despite its significant increase compared to a typical mask filter, is acceptable considering the pressure drop of N95 masks available in the market.[25]

3.2.3. Gas rejection. The main advantage of modified filters with polystyrene and nano-composite fibers is their efficiency in removing air pollutants such as NO_2, CO_2, and SO_2, which are among the main components of air pollution and are of particularly important. In the following, the performance of filters in removing these gases separately was examined.

3.2.3.1. CO_2 rejection. The diagram in Fig. 6 shows the performance of fibrous filters in removing CO_2 gas, which was prepared by two methods of solution and stabilization. As it is clear in the figure, with the increase in the percentage of KCC-1, the performance of the fibers in removing CO_2 gas has improved, and also, the nano-composite fibers prepared by the stabilized method have performed better in this test as in other tests, and the best performance was related to the fibers containing KCC-1 and ZnO NPs (89%). The nanostructures present in modified nanocomposite filters were actively able to absorb CO_2 gas, which occurs through physical or chemical surface adsorption *via* functional groups on KCC-1.

3.2.3.2. SO_2 rejection. The performance of fiber masks in removing SO_2 gas is shown in Fig. 7. The weakest performance in removing gases is related to SO_2 gas. As can be seen, the efficiency of nanocomposite filters has significantly increased compared to filters without nanostructures. On the other hand, the removal performance has improved with the increase in the percentage of KCC-1. In this test, modified filters with nanocomposite fibers had the best performance in terms of the stabilized method, and the best performance was related to fibers containing both KCC-1 and ZnO NPs with an 83% removal rate.

3.2.3.3. NO_2 rejection. The performance of fiber masks in removing NO_2 gas is shown in Fig. 8. In this test, the removal performance improved with the increase in the percentage of KCC-1. Similar to previous tests, the best performance was related to nanocomposite fibers prepared by the stabilized method, and the best performance was related to fibers containing both KCC-1 and ZnO NPs, which was justifiable considering the effect of both nanostructures in absorption. The reduction in the absorption rate of this pollutant compared to other pollutants is related to better interactions between the absorbent and other absorbed pollutants (CO_2 and SO_2), which are influenced by the type of functional groups, the type of interactions created, as well as the size of the absorbent pores and the size of the absorbed particles.[26]

Removal of gases in filters can be done through different mechanisms. The filters have a layer consisting of fibers with a diameter of approximately 1 micrometer on their surface, which form a porous barrier and can remove some of the gases with a sieving mechanism. On the other hand, these fibers contain stabilized KCC-1 nanostructures, which is a porous material and has several functional groups due to the dendrimer structure. Fibers with these nanostructures, having a high surface-to-volume ratio, can act as active gas adsorbents.

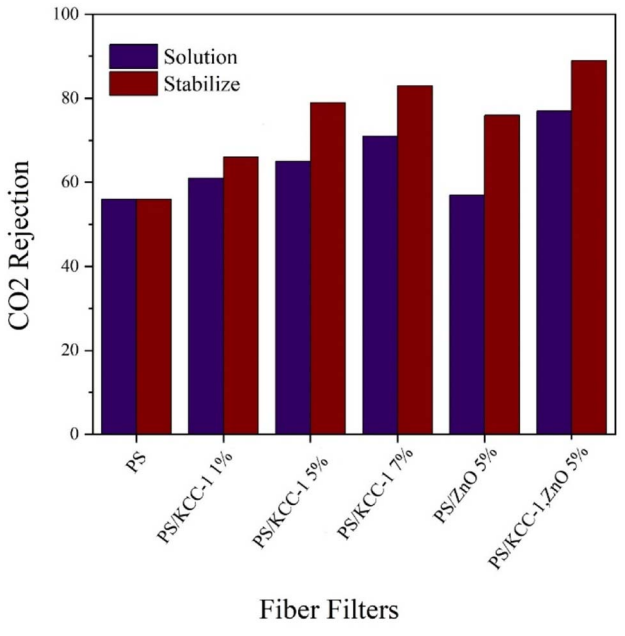

Fig. 6 CO_2 rejection of PS fibers and PS-nanocomposite fibers.

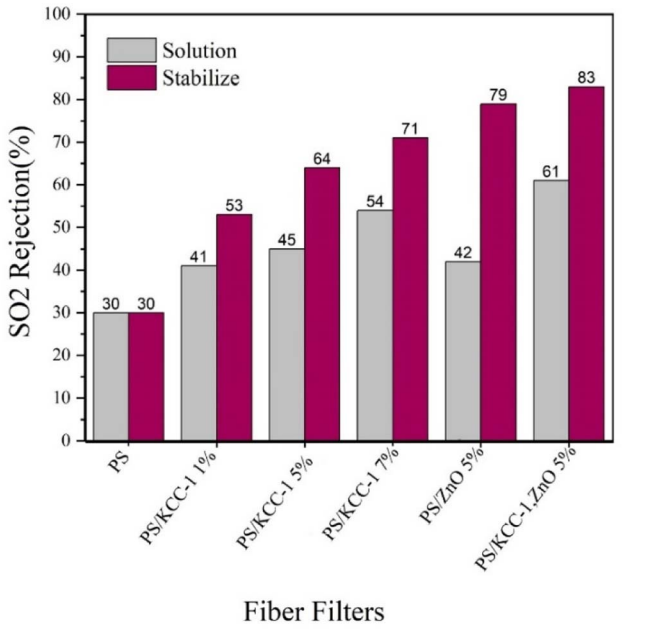

Fig. 7 SO_2 rejection of PS fibers and PS-nanocomposite fibers.

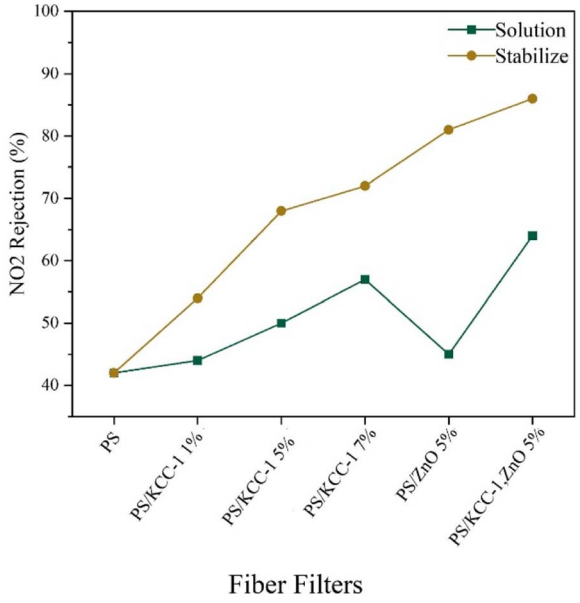

Fig. 8 NO_2 rejection of PS fibers and PS-nanocomposite fibers.

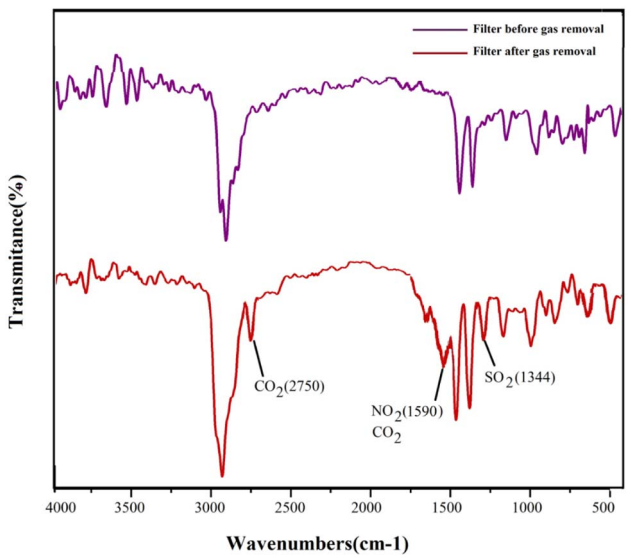

Fig. 9 FT-IR spectra of PS/KCC-1, ZnO filter before and after gas removal.

The interaction of gases with KCC-1 functional groups will also be effective in absorbing gases.

To confirm the adsorption of gases by the surface fibrous filter, the optimal filter used for the adsorption of gases (stabilized PS/KCC-1, ZnO) was studied by FT-IR analysis. The resulting spectrum of this filter before and after use is shown in Fig. 9. As can be seen, new peaks have appeared in the spectrum related to the filter used to remove gases, at 1344, 1590 and 2750 cm^{-1}, which were related to the bending vibrations of the O–S bond[27] and the stretching vibrations of the carbonate and bicarbonate salts[28] and the N–O bonds.[29]

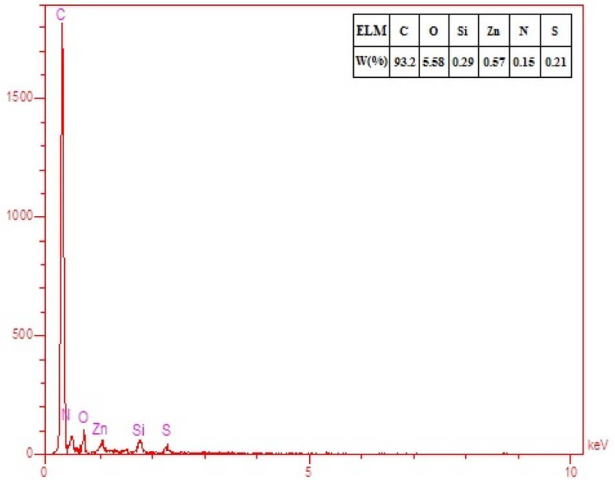

Fig. 10 EDS elemental analysis of PS/KCC-1, ZnO filter after gas removal.

To further prove the presence of elements in the adsorbed gases on the filter surface, EDS elemental analysis was performed, and the result is shown in Fig. 10. It was observed that nitrogen and sulfur were detectable on the surface of the sample and this indicated the adsorption of NO_2 and SO_2 by the filter.

The studies conducted on hybrid nanocomposite fibrous filters are minimal and, most of the published articles have focused on pressure drop and removal efficiency of suspended particles. The investigation of gas removal is limited to this article, and no reference was found for comparison with other studies. In Table 2, the results obtained in this study have been compared with other reports. As can be seen, the removal efficiency of suspended particles in this study was close to 100%, and almost all suspended particles have been removed. The reported pressure drops (despite being high) was within the range reported in other articles and was acceptable. Gas removal was also performed with an efficiency higher than 80%.

3.3. Antibacterial tests

Considering the presence of ZnO nanomaterials in the modified fiber filter (sample M5), the antibacterial activity of this sample was studied and compared to the sample without ZnO. In this test, bacteria were grown in parallel strips, and the samples were placed on these strips. A commercial mask filter was used as the control sample in this test. The results of the antibacterial activity test for *E. Nreus* (Gram-positive bacteria) and *E. coli* (Gram-negative bacteria) are presented in Fig. 11. The PS fiber filter did not prevent the growth of bacteria. However, the nanocomposite filter containing ZnO NPs inhibited the growth of both types of bacteria. This inhibition was limited to the contact surface between the nanocomposite fibers and the bacteria. In contrast, complete bacterial growth was observed under sterile gas in the control group. These findings confirmed the antibacterial effect of the filter containing ZnO NPs, while the polystyrene fiber-modified filter did not prevent the growth of bacteria.

Table 2 Comparison removal performance of constructed filter with previous reports

Mask name	PM2.5 removal (%)	Pressure drop (Pa)	Removal of gases (%)			Reference
			CO_2	SO_2	NO_2	
PS/KCC-1, ZnO fibers	99.1	180	89	83	86	This research
N95	95	343	—	—	—	25
Graphene oxide nanocomposite mask	99.9	100	—	—	—	30
MNP-NF filters	99	269	—	—	—	31
PS/acid-treated cellulose nanocrystals	99	231	—	—	—	13
PBS fibers and PBS nanofibers	98	59	—	—	—	32
Polyacrylonitrile/ZnO nanofiber	98	48	—	—	—	11
PAN/TiO_2 beads/P25	88	96.75	—	—	—	33
Polyacrylonitrile/silver nanofiber	99	33	—	—	—	34

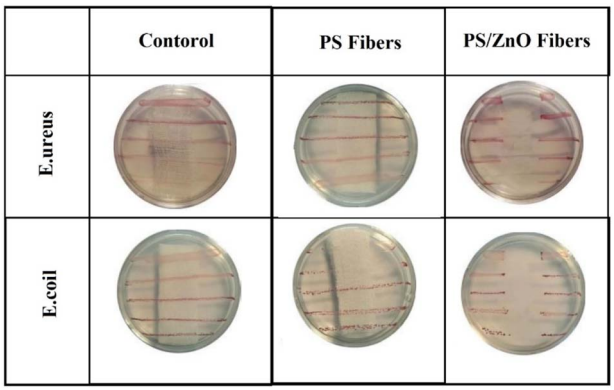

Fig. 11 Antibacterial tests of PS fibers and PS/ZnO fibers.

4. Conclusion

This research has shown that the efficacy of respiratory masks in filtering air pollutants can be significantly enhanced by incorporating polystyrene fibers, KCC-1, and ZnO NPs. Analytical techniques confirmed the attachment of NPs to the polymer fibers on the filter surface, and filtration tests demonstrated that filters prepared with a superior fixation method exhibited the highest efficiency in removing suspended particles and various gases. Furthermore, nanocomposite fibers containing ZnO NPs displayed antibacterial properties, inhibiting the growth of both Gram-positive and Gram-negative bacteria. Therefore, the integration of these advanced nanomaterials into respiratory masks has the potential to bolster their protective capacity against air pollutants and contribute to public health improvements.

Author contributions

Conceptualization: NS and MM. Data curation: MA. Formal analysis: MM and NS. Investigation: FE. Methodology: MM and NS. Project administration: NS. Supervision: NS. Validation: NS and MM. Writing – original draft: FE, MM, and NS. Writing – review & editing: MA, MM, and NS.

Conflicts of interest

There are no conflicts to declare.

Acknowledgements

This research was supported by Urmia University. We gratefully acknowledge the support of this work by Urmia University, Urmia, Iran.

References

1 Z. Zhang, G. Zhang and B. Su, *Socio-Econ. Plan. Sci.*, 2022, **83**, 101167.
2 S. Mallakpour, E. Azadi and C. M. Hussain, *Adv. Colloid Interface Sci.*, 2022, **303**, 102653.
3 M. Z. Rahman, M. E. Hoque, M. R. Alam, M. A. Rouf, S. I. Khan, H. Xu and S. Ramakrishna, *Polymers*, 2022, **14**, 1296.
4 Y. A. Attia, A. E. Ezet, S. Saeed and A. H. Galmed, *Sci. Rep.*, 2024, **14**, 621.
5 V. Babaahmadi, H. Amid, M. Naeimirad and S. Ramakrishna, *Sci. Total Environ.*, 2021, **798**, 149233.
6 M.-L. Wang, D.-G. Yu and S. W. A. Bligh, *Appl. Mater. Today*, 2023, **31**, 101766.
7 N. Angel, S. Li, F. Yan and L. Kong, *Trends Food Sci. Technol.*, 2022, **120**, 308–324.
8 M. Zahmatkeshan, M. Adel, S. Bahrami, F. Esmaeili, S. M. Rezayat, Y. Saeedi, B. Mehravi, S. B. Jameie and K. Ashtari, in *Handbook of Nanofibers*, Springer, 2019, pp. 215–261.
9 B. Singh, J. Na, M. Konarova, T. Wakihara, Y. Yamauchi, C. Salomon and M. B. Gawande, *Bull. Chem. Soc. Jpn.*, 2020, **93**, 1459–1496.
10 M. Anvari Gharabaghlou, N. Shadjou and A. Poursattar Marjani, *Appl. Organomet. Chem.*, 2020, **34**, e5868.
11 J. H. Kim, G. H. Lee, J. Ma, S. Lee and C. S. Kim, *J. Colloid Interface Sci.*, 2022, **612**, 496–503.
12 S. Ullah, A. Ullah, J. Lee, Y. Jeong, M. Hashmi, C. Zhu, K. I. Joo, H. J. Cha and I. S. Kim, *ACS Appl. Nano Mater.*, 2020, **3**, 7231–7241.
13 D. Wong, S. Hartery, E. Keltie, R. Chang, J. S. Kim and S. S. Park, *ACS Appl. Polym. Mater.*, 2021, **3**, 4949–4958.
14 H. Tang, D. Han and J. Zhang, *Nano Express*, 2021, **2**, 020017.
15 J. Soleymani, M. Hasanzadeh, M. H. Somi, N. Shadjou and A. Jouyban, *Biosens. Bioelectron.*, 2019, **132**, 122–131.

16 A. Belay, B. Bekele and A. C. Reddy, *Dig. J. Nanomater. Bios.*, 2019, **14**, 3941923.
17 H. S. Oboudatian and J. Safaei-Ghomi, *Sci. Rep.*, 2022, **12**, 2381.
18 D. Damberga, V. Fedorenko, K. Grundšteins, Ş. Altundal, A. Šutka, A. Ramanavičius, E. Coy, R. Mrówczyński, I. Iatsunskyi and R. Viter, *Nanomaterials*, 2020, **10**, 2438.
19 Z. Dong, X. Le, X. Li, W. Zhang, C. Dong and J. Ma, *Appl. Catal., B*, 2014, **158**, 129–135.
20 A. C. Janaki, E. Sailatha and S. Gunasekaran, *Spectrochim. Acta, Part A*, 2015, **144**, 17–22.
21 S. K. Sen, U. C. Barman, M. Manir, P. Mondal, S. Dutta, M. Paul, M. Chowdhury and M. Hakim, *Adv. Nat. Sci.: Nanosci. Nanotechnol.*, 2020, **11**, 025004.
22 T. Nitanan, P. Opanasopit, P. Akkaramongkolporn, T. Rojanarata, T. Ngawhirunpat and P. Supaphol, *Korean J. Chem. Eng.*, 2012, **29**, 173–181.
23 Y. A. Sihombing, M. Z. E. Sinaga, R. Hardiyanti and I. R. Saragi, *Heliyon*, 2022, **8**(8), e10113.
24 M. A. H. Hamdan, N. H. H. Hairom, N. Zaiton, Z. Harun, C. F. Soon, S. K. Hubadillah, M. R. Jamalludin, N. W. C. Jusoh and A. A. Jalil, *Emerging Advances in Integrated Technology*, 2021, **2**, 30–38.
25 L. Cassorla, *Anesthesia and Analgesia*, 2020.
26 H. S. Park, D. Kang, J. H. Kang, K. Kim, J. Kim and H. Song, *Int. J. Environ. Res. Public Health*, 2021, **18**, 597.
27 Y. Hwang, A. Farooq, H. W. Lee, S.-H. Jang, S. H. Park, M.-H. Lee, S. C. Choi and Y.-K. Park, *J. Hazard. Mater.*, 2020, **397**, 122581.
28 J. M. Dorhout, A. S. Anderson, E. Batista, R. K. Carlson, R. P. Currier, R. K. Martinez, S. M. Clegg, M. P. Wilkerson and K. Nowak-Lovato, *J. Mol. Spectrosc.*, 2020, **372**, 111334.
29 F. Azzolina-Jury and F. Thibault-Starzyk, *Top. Catal.*, 2017, **60**, 1709–1721.
30 W. Jung, J. S. Lee, S. Han, S. H. Ko, T. Kim and Y. H. Kim, *J. Mater. Chem. A*, 2018, **6**, 16975–16982.
31 J. Kim, S. Chan Hong, G. N. Bae and J. H. Jung, *Environ. Sci. Technol.*, 2017, **51**, 11967–11975.
32 S. Choi, H. Jeon, M. Jang, H. Kim, G. Shin, J. M. Koo, M. Lee, H. K. Sung, Y. Eom and H. S. Yang, *Advanced Science*, 2021, **8**, 2003155.
33 K.-N. Chen, F. N. I. Sari and J.-M. Ting, *Appl. Surf. Sci.*, 2019, **493**, 157–164.
34 M. Sohrabi, M. Abbasi and A. Sadighzadeh, *Polym. Bull.*, 2023, **80**, 5481–5499.